Research Square

Preprints are preliminary reports that have not undergone peer review.
They should not be considered conclusive, used to inform clinical practice,
or referenced by the media as validated information.

Acceleration of Esophageal Wound Healing by Anisotropically Aligned Smooth Muscle Cell-Laden Nanofibrous Patch

Miji Yeo
Sungkyunkwan University (SKKU)
Jung Won Yoon
Pusan National University
Gyu Tae Park
Pusan National University
Sung-Chan Shin
Pusan National University and Medical Research Institute, Pusan National University Hospital
Young-Cheol Song
Pusan National University
Yong-Il Cheon
Pusan National University and Medical Research Institute, Pusan National University Hospital
Byung-Joo Lee
Pusan National University and Medical Research Institute, Pusan National University Hospital
Geun Hyung Kim
Sungkyunkwan University (SKKU)
Jae Ho Kim (jhkimst@pusan.ac.kr)
Pusan National University

Research Article

Keywords: cell electrospinning, smooth muscle cells, mesenchymal stem cells, differentiation, esophageal reconstruction

Posted Date: April 27th, 2022

DOI: https://doi.org/10.21203/rs.3.rs-1558901/v1

License: This work is licensed under a Creative Commons Attribution 4.0 International License.
Read Full License

Abstract

Esophageal tissue engineering is proposed to repair damaged esophagus, which requires peristalsis *via* directional alignment and movement of smooth muscle. Cell electrospinning is an effective technique to produce aligned muscle tissues by directly encapsulating living cells into micro/nanofibers. Mesenchymal stem cells (MSCs) can differentiate into smooth muscle cells (SMCs) in response to treatment with transforming growth factor-β1. In this study, cell electrospinning or three dimensional bioprinting were used to generate anisotropic or random alignment of MSCs and MSC-derived SMCs. Cell electrospinning resulted in more aligned and elongated forms of MSCs and SMCs than bioprinting. SMCs aligned *via* cell electrospinning exhibited upregulated expression of SMC-specific markers (alpha-smooth muscle actin, calponin, SM22α, and desmin), SMC-associated extracellular matrix proteins (fibronectin, collagen types I and IV), and connexin 43, the principal gap junction protein in SMCs. The electrospun SMC was fabricated in a patch form and transplanted into a rat esophageal defect model. Transplantation of the smooth muscle patch promoted muscle regeneration and vascularization in esophageal wounds. Taken together, these results suggest that transforming growth factor-β1-induced differentiation of MSCs to SMCs and anisotropic alignment of SMCs can be applied to engineer smooth muscle tissues and treat gastrointestinal perforation.

Introduction

The esophagus is a tubular organ that extends from the epiglottis in the pharynx to the stomach. This organ is composed of thin, elongated smooth muscle cells (SMCs) aligned in parallel to one another along one direction for contractile function. When food is swallowed, the esophagus pushes the ingested food bolus toward the stomach *via* peristalsis, which is mediated by the contraction of circular and longitudinal esophageal muscles [1]. Esophageal diseases such as congenital defects and esophageal cancer cause circumferential, full-thickness, and extended segment loss of the esophagus. Gastric pull-up conduits or colon interpositions are usually used to treat esophageal perforations. However, these esophageal substitutes have shown limited success and are typically associated with significant mortality [2]. Therefore, esophageal tissue engineering has attracted attention as a promising strategy for regenerating a patient's native esophagus [3]. However, no positive evidence that engineered esophageal tissue can mimic the structural and functional characteristics of smooth muscle in the esophagus is available to-date. Recently, stem cell-based tissue engineering has emerged as a potential method for improving the therapeutic efficacy of engineered tissues through the construction of endogenous cell types.

Mesenchymal stem cells (MSCs) can differentiate into multiple cell lineages, including adipocytes, osteoblasts, chondrocytes, skeletal myocytes, and SMCs [4–6]. Transforming growth factor-β1 (TGF-β1) is a potent inducer of MSC and SMC differentiation *via* the activation of the TGF-β-SMAD signaling cascade [7, 8]. Studies have shown that TGF-β1 treatment increases the expression of SMC-specific ion channels in human adipose-derived MSCs [9]. In addition to extracellular stimuli, cell alignment through micropatterning has been reported to increase the expression of F-actin and alpha smooth muscle actin

(α-SMA) in SMCs and promote the contractile phenotype [10, 11]. However, direct transplantation of SMCs into damaged tissues does not support cell alignment, which is critical for contractile function in smooth muscle tissues. Therefore, several strategies have been developed to guide cell alignment, including the use of aligned substrates and electrospun fibers [12, 13]. However, there remains a critical need to develop novel methods to fabricate smooth muscle tissues with aligned structures in three dimensions (3D).

Cellular topography has been reported to regulate cell adhesion, cytoskeletal organization, and cell-cell connection and play a key role in the lineage specification of stem cells [14, 15]. Cells sense surface patterns and different kinds of nanoscale stimuli. Submicron topography regulates various stem cell responses, including proliferation, migration, and differentiation [16] by changing focal adhesion assembly, which causes variations in cytoskeletal organization and cell mechanical properties [17]. Therefore, topographical features such as anisotropic patterning, nanostructure, and fibrillar structure, could play a significant role in spatial organization during myogenesis [18–20]. It has been shown that a microgrooved topography with stiff substrates stimulates the differentiation of MSCs into SMCs [21]. Moreover, microgrooved topography and TGF-β1 treatment cooperatively stimulate the expression of SMC-specific contractile proteins in MSCs [22]. However, topographic modulation for esophageal tissue engineering using MSCs has not yet been studied.

3D bioprinting is an emerging technique to fabricate a 3D tissue that can mimic an organ, but it has proved difficult to generate the topographic features of the cells constituting the tissue [23, 24]. Cell electrospinning (CE) is an advanced technique that directly encapsulates living cells in micro/nanofibers. This process overcomes the restrictions of 3D nutrition accessibility and cell distribution in the entire depth of the scaffold, which is an intrinsic limitation of conventional electrospinning [25]. Various cell types, such as neuroblastoma cells, cardiac myocytes, osteoblasts, and adipose stem cells, have been utilized for CE [25–28]. Furthermore, we previously demonstrated that the arrangement of myoblasts and human umbilical vein endothelial cells could be induced by CE [29, 30]. However, whether CE can be applied to engineer aligned smooth muscle of esophageal tissues has not been explored.

To explore whether CE affects the differentiation of MSCs into aligned SMCs, we compared the effects of CE and cell printing (CP) in combination with TGF-β1 treatment on the differentiation of MSCs into aligned SMCs. Moreover, we examined the therapeutic application of an aligned smooth muscle sheet to repair esophageal wounds.

Materials & Methods

Materials

α-Minimum Essential Medium (α-MEM), Hank's balanced salt solution (HBSS), fetal bovine serum (FBS), and trypsin-EDTA were purchased from Invitrogen (Carlsbad, CA, USA). TGF-β1 was purchased from Peprotech (Cranbury, NJ, USA). Smooth muscle growth medium-2 (SmGM^{TM}-2) was purchased from

Lonza (Bazel, Switzerland). Polycaprolactone (PCL; molecular weight (M_w) = 45,000 Da), calcium chloride ($CaCl_2$), and polyethylene oxide (PEO; M_w = 900,000) were purchased from Sigma-Aldrich (St. Louis, MO, USA). Sodium alginate with 0.42 mannuronic acid to guluronic acid (M/G) ratio (LF10/60; FMC Biopolymer, Drammen, Norway) was kindly provided by Pharmaline (Suwon, South Korea). 4',6-diamidino-2-phenylindole (DAPI) was purchased from Merck (Darmstadt, Germany). The antibodies used in this study are listed in Table S1.

Isolation of MSCs from human palatine tonsil tissues and cell culture

After obtaining informed consent from patients, human palatine tonsil tissues were isolated from patients undergoing tonsillectomy due to chronic tonsillar hypertrophy and/or chronic tonsillitis in the Department of Otorhinolaryngology-Head and Neck Surgery, Pusan National University Hospital [31, 32]. To isolate tonsil-derived MSCs, tonsil tissues were washed with phosphate-buffered saline (PBS) and digested at 37°C for 30 min with 0.075% type I collagenase. The enzyme activity was neutralized with α-MEM supplemented with 10% FBS and 10% penicillin-streptomycin. The dissociated cells were filtered through a sterile 70 μm cell strainer and cultured in 5% CO_2 at 37°C. When the cell confluence reached 70–80%, cells were washed twice with HBSS, treated with 0.05% trypsin-EDTA, and incubated in 5% CO_2 at 37°C for 3–5 min. The suspended cells were harvested in medium containing FBS and centrifuged at 500 × *g* for 4 min. MSCs were sub-cultured at a split ratio of 1:3 or 1:4, and cells at passage 7–9 were used for experiments. To differentiate MSCs into SMCs, MSCs were serum-starved in α-MEM basal media for 24 h, treated with 2 ng/mL TGF-β1 for 4 days, and maintained in SmGM^{TM}-2 medium.

Western blotting

To extract total protein, cells were treated with lysis buffer [Tris-HCl (20 mM), EGTA (1 mM), EDTA (1 mM), NaCl (10 mM), phenylmethylsulfonyl fluoride (0.1 mM), Na_3VO_4 (1 mM), sodium pyrophosphate (30 mM), β-glycerol phosphate (25 mM), and 1% Triton X-100, pH 7.4], followed by sonication and centrifugation at 12,000 rpm at 4°C for 10 min. Lysates were resolved using sodium dodecyl sulfate-polyacrylamide gel electrophoresis and transferred onto nitrocellulose membranes. The membranes were blocked with 5% skim milk buffer for 2 h and incubated overnight with primary antibodies. For visualization with chemiluminescence, the membranes were incubated with horseradish peroxidase-conjugated secondary antibodies for 1 h, and the signal was detected with the ECL kit (Cytiva, Mariborough, MA). The membrane was washed four times for 20 min with 1× Tris-Tween buffered saline.

Cell growth on two-dimensional (2D) surface with/without aligned fibers

A rectangular glass (10 × 10 mm) was used as the non-fibrous surface. Then, aligned alginate fibers were deposited by electrospinning onto the glass under a 10.5 kV high-voltage power source, 140 mm nozzle-to-electrode (NtE) distance, 0.25 mL/h flow rate, and 3 min electrospun time. The fibers were aligned using rectangular copper electrodes (75 × 25 mm) and a metal nozzle (180 μm). Then, MSCs and SMCs

at 62500 cells/droplet, which is mathematically equivalent to the number of cells laden on the CE scaffold, were seeded on the glass with or without aligned fibers.

Preparation of cell-laden bioink

To obtain a cell-laden bioink, 2 wt % alginate and 3 wt % PEO (A2P3) were dissolved in triple-distilled water and stirred for 2 days at 4°C. Then, either MSCs or SMCs at 1×10^7 cells/mL were added to the A2P3 solution.

Fabrication of cell-printed and cell-electrospun scaffold using MSCs and SMCs

A 3D printer (DTR3-2210-T-SG, DASA Robot, Bucheon, South Korea) was used to fabricate a PCL strut (300 μm in diameter and 30 mm in length). Pneumatic pressure (340 kPa) was applied within the heated metal barrel containing PCL at 100°C, and the melted PCL was extruded through a metal nozzle (350 μm inner diameter (ID)) at 10 mm/s. CP was subsequently performed on printed PCL struts. The cell-laden bioink was printed through a nozzle (ID: 180 μm) using a pneumatic pressure of 120 kPa and a nozzle moving speed of 10 mm/s.

For CE, a high-voltage power source (SHV300RD-50K, Convertech, Gwangmyeong, South Korea) and a syringe pump (KDS 230, NanoNC, Inc., Seoul, South Korea) were prepared. The cell-laden bioink was supplied at 0.25 mL/h, and electrospun under a 10.5 kV high voltage direct current (HVDC) and 140 mm NtE distance. The electrospun fibers were deposited on the PCL strut, which was fixed between parallel cylindrical electrodes at a distance of 30 mm.

To fabricate a PCL fibrous mat, electrospinning was performed using 10% PCL dissolved in methylene chloride and dimethylformamide at a 4:1 ratio. The PCL fibers were collected on a grounded rotating drum at 1500 rpm using 0.20 mL/h flow rate and 0.1 kV/mm electric field (12 kV HVDC and 120 mm NtE distance) for 4 h.

Characterization of the surface topography of scaffolds

To observe the surface topography of the scaffolds, optical images were captured using a BX FM-32 optical microscope (Olympus, Japan). To obtain microscale images, the samples were placed on double-sided carbon tape and sputter-coated with gold, and their images were captured using a scanning electron microscope (SEM; SNE-3000M; SEC Inc., Suwon, South Korea). Stress-strain curves were obtained using a microtensile tester (Toptech 2000; Chemilab, Suwon, South Korea) under uniaxial stretching at 0.2 mm/s.

Analysis of cell viability and differentiation on cell-laden scaffolds

Cell viability at various cell culture periods (*in situ*, 7, 14, and 21 days) was observed using a Live/Dead Viability/Cytotoxicity Kit (Invitrogen). The samples were immersed in a solution containing 0.15 mM

calcein AM and 2 mM ethidium homodimer-1 for 30 min, and images were captured using light microscopy. Cell viability was calculated as the ratio of the number of live cells to the total cell number using Fiji software.

Cell nuclei and F-actin were visualized with DAPI (blue) and phalloidin (green) staining, respectively. The samples were fixed in formaldehyde solution (3.7% in Tris-buffered saline [TBS]) for 12 h at 4 ^{o}C and treated with 0.3% Triton X-100 in TBS for 10 min at 25 ^{o}C. Then, the samples were treated for 1 h at 37 ^{o}C with a DAPI (5×10^{-6} M; Invitrogen)/phalloidin (15 U/mL; Invitrogen) staining solution. Fluorescence images were captured using a confocal microscope (LSM 700; Carl Zeiss, Germany) and analyzed using Fiji software.

Differentiation of MSCs and SMCs was observed using immunofluorescence staining. Samples were fixed and permeabilized prior to DAPI/phalloidin staining. The samples were then immersed in 1% bovine serum albumin (BSA) in TBS for 1 h at room temperature. Primary antibodies against α-SMA, fibronectin, calponin, collagen I, and collagen IV at 1:200 in TBS were added to the samples and incubated overnight at 4 ^{o}C. Subsequently, the samples were stained with secondary antibodies conjugated with Alexa Fluor 488 or 594 (Invitrogen). Images were captured using confocal microscopy and analyzed using Fiji software.

Reverse transcription-quantitative polymerase chain reaction (RT-qPCR)

The expression levels of connexin 43 (*Cx43*), smooth muscle protein 22 alpha (*SM22α*), desmin, and smoothelin (*SMTN*) were analyzed using RT-qPCR. Briefly, total RNA was isolated using TRI reagent (Sigma-Aldrich) according to the manufacturer's instructions. The purity and concentration of the isolated RNA were determined using a spectrophotometer (FLX800T; Biotek, VT, USA). cDNA synthesis was performed using 500 ng RNase-free DNase-treated total RNA using a reverse transcription system (FSQ-201; Toyobo, Osaka, Japan). The gene expression level was measured by the comparative C_t method using the StepOne Plus RT-PCR system (Applied Biosystems, Foster City, CA, USA). *GAPDH* gene expression was used as an internal control. The primers used in this study are listed in Table S2.

Repair of esophageal wounds using SMC-laden patch

Six-month-old Sprague-Dawley rats (Central Lab. Animal Inc., Seoul, Korea), weighing approximately 680–700 g, were used in this study. Rats were anesthetized with isoflurane (Baxter International Inc., USA). An anesthetic delivery equipment was used to administer a gas mixture of isoflurane and O_2 via inhalation into the rat's respiratory system. Before anesthesia, isoflurane was evaporated in a vaporizer (Harvard Apparatus, USA), and the concentration was set to 5% and adjusted to 2% during the operation. The gas flow rate of O_2 was maintained at 0.5–1 LPM.

To create an esophageal defect model, the center of the ventral neck was shaved, an incision of approximately 2 cm made, and the esophagus located in the tracheoesophageal structure. To equalize

the size of the esophageal defect, a biopsy punch (Miltex, KAI Industries, Japan) of 2 mm diameter was used to completely puncture the muscle and mucosa layer of the esophagus. The patches were cut with a biopsy punch of 4 mm diameter and placed over the esophageal defect, and the punctured section of the esophagus was sutured with a 9 – 0 nylon suture (AILEE Co., Korea). The incised skin was sutured using a 7 – 0 nylon suture. All surgical procedures were performed using sterile instruments and disinfection procedures. Fasting was abstained for 3 days after surgery, sterilized water was fed on the 4th day, and food was served on the 6th day. Two weeks after the surgery, the rats were sacrificed by CO_2 euthanasia. All experiments were reviewed and approved by the Institutional Review Board of Pusan National University Hospital (PNUH-2021-188).

Histological analysis

For histological analysis of esophageal regeneration, esophageal tissues were excised with tracheal tissue to support the esophagus. For routine staining, the tissues were fixed with cooled acetone. To obtain cryosections, the tissue was perfused with sucrose solution, embedded in optimal cutting temperature compound, and frozen at -80°C. For routine staining, the tissue sections were stained with hematoxylin and eosin (H&E) and Masson's trichrome stain. Stained sections were scanned using an Axio Scan.Z1 (Carl Zeiss Microscopy, Germany).

For immunohistochemical analysis, the tissue samples were fixed in 4% paraformaldehyde overnight and embedded in paraffin. To detect smooth muscle regeneration and vascularization, esophageal tissue sections were stained with anti-SM22α, anti-IL-B4, anti-vimentin, and anti-desmin antibodies. Macrophages were stained using anti-CD68 antibody. Alexa Fluor 568 goat anti-mouse and Alexa Fluor 488 goat anti-mouse antibodies and Alexa Fluor 488 streptavidin were used to label the fluorescence, and DAPI was used to stain the nuclei. The stained sections were visualized under a laser confocal microscope (Olympus FluoView FV1000) and Axio Scan.Z1 (Carl Zeiss Microscopy). The fluorescence levels were quantified in a high-power field using ImageJ software.

Statistical analysis

The data are presented as the mean ± standard deviation and were analyzed using SPSS 18 software (SPSS, Inc., Chicago, IL, USA). Differences among multiple groups were compared using analysis of variance, and the statistical significance was represented as $p^* < 0.05$, $p^{**} < 0.01$, and $p^{***} < 0.001$.

Results

Cell printing and cell electrospinning of MSCs and SMCs

The differentiation of MSCs into SMCs *in vitro* was induced by treating MSCs with TGF-β1 and analyzed using western blotting. TGF-β1 treatment increased the expression of several SMC markers, including calponin, α-SMA, SM22α, vimentin, desmin, and smoothelin, indicating the differentiation of MSCs into SMCs (Fig. S1). Next, we compared the effects of CE and 3D CP on the anisotropic alignment of MSCs and MSC-derived SMCs. The bioink was prepared by mixing a 2 wt % alginate/3 wt % PEO (A2P3)

solution and live MSCs and SMCs at 1×10^7 cells/mL. Alginate is a biocompatible, nontoxic, and versatile polymer that enables rapid gelation of the microstructure through the addition of cations [33]. PEO was added as a processing material to optimize the surface tension, conductivity, and molecular entanglement for electrospinning [34]. The composition of A2P3 was selected from a previous study which showed considerable fiber formation and alignment [29]. As shown in Fig. 1A, CP and CE were performed with cells and bioink according to the schematic illustration. In the optical images, CE scaffold has a fibrous structure, whereas CP scaffold has a bulk structure. The morphology of SMCs was confirmed by Phalloidin/DAPI staining after 7 days of culturing. The cells of CP scaffold had a round shape similar to that of day 0, whereas the cells of CE scaffold exhibited elongated morphology. However, these scaffolds have a low mechanical strength, which can easily bend and deform, providing an unstable environment for a long-term cell culture. Therefore, PCL strut was applied as a mechanical support for CP and CE scaffolds. 3D CP was performed using a pneumatic pressure of 340 kPa and nozzle moving speed of 10 mm/s yielding a 300 μm PCL strut (Fig. 1B (i)). MSCs and SMCs were printed onto the PCL struts using 120 kPa pneumatic pressure and 10 mm/s nozzle moving speed and were referred to as CP-MSC and CP-SMC, respectively (Fig. 1B (ii)). To produce aligned smooth muscle scaffolds, the PCL struts were subjected to MSC and SMC-laden electrospinning using a 140 mm NtE distance, 0.075 kV/mm electric field, and 0.25 mL/h flow rate (Fig. 1B (iii)). The scaffolds derived by CE of MSCs and SMCs were referred to as CE-MSC and CE-SMC, respectively.

Topographical features of the scaffolds fabricated *via* CP and CE were evaluated by optical and SEM imaging. This analysis revealed that CP scaffolds exhibited smooth surfaces, whereas the CE fibers displayed aligned micropatterns (Fig. 1C, D). To test whether the MSCs and SMCs were compatible with the fabrication processes, the cell viability of the scaffolds was measured. The results showed high initial cell viability (> 90%) of MSC- and SMC-laden scaffolds (Fig. 1E), indicating that both CP and CE structures provided a biocompatible microenvironment for MSCs and SMCs.

Cell compatibility of cell printed and cell electrospun scaffolds

To explore whether cell proliferation was affected by CP and CE, we measured cell viability after culturing for longer periods. Figure 2A shows the live (green color) and dead (red color) cells after 7, 14, and 21 days of culturing. As shown in Fig. 2B, most of the cells remained viable after 21-day-incubation of CE and CP scaffolds (Fig. 2B). The number of cells at day 21 was counted from the images of the live/dead assay (Fig. 2C). CE-SMC had the highest cell number compared to that of other scaffolds, suggesting that cell alignment promoted proliferation of SMCs.

Effects of cell printing and electrospinning on differentiation of MSCs to SMCs

It has been previously reported that cell elongation promotes the differentiation of MSCs into SMCs [12, 35], and cell morphologies affect the phenotypic modulation of SMCs [36]. We examined the effects of CP and CE on the cell morphology and phenotypes of MSCs and SMCs. After fabricating aligned fibers on a glass surface, MSCs and SMCs were seeded (Fig. S2A). As a control, a glass without fibers was used. MSCs and SMCs cultured on glass containing aligned fibers exhibited increased cell elongation and cell alignment compared to that of those cultured on glass without fibers. Additionally, MSCs and SMCs cultured on aligned fibers displayed increased expression of SMC markers (α-SMA and calponin) and SMC-related extracellular matrix (ECM) markers (collagen I, collagen IV, and fibronectin) (Fig. S2B-D). Furthermore, the differentiation of MSCs into SMCs and maturation of SMCs were promoted by cell elongation in 2D. Therefore, CE of MSCs and SMCs was performed to obtain aligned fibers and develop a smooth muscle regenerative scaffold in 3D.

Figure 3A shows the Phalloidin/DAPI staining of CP and CE MSCs and SMCs. The CP scaffolds (CP-MSC and CP-SMC) contained cells with multipolar morphology, while the CE scaffolds (CE-MSC and CE-SMC) contained anisotropically aligned spindle-shaped cells. These features were analyzed quantitatively with respect to the F-actin aspect ratio and orientation factor (Fig. 3B, C). This analysis showed that both the F-actin aspect ratio and orientation factor were greatly increased on CE scaffolds. The expression and distribution patterns of ECM components, such as fibronectin, collagen I, and collagen IV, are shown in Fig. 3D. Fibronectin has been reported to enhance cell migration [37], whereas collagen provides mechanical strength to prevent tissue failure [38]. CE-SMC showed enhanced expression of all three ECM components (fibronectin, collagen I, and collagen IV) (Fig. 3E).

CP-MSCs and CE-MSCs exhibited very low expression of α-SMA, but nonetheless had a well-represented cytoskeletal structure (Fig. 4A). The expression levels of α-SMA in CP-SMC and CE-SMC were increased by at least 3-fold compared to those in MSCs (Fig. 4B). Additionally, the α-SMA orientation factor was highly expressed in CP-MSCs and CE-MSCs owing to the presence of aligned topographical cues (Fig. 4C). Calponin, a smooth muscle-specific protein expressed in the late stage of differentiation, showed significantly higher expression in SMCs than in MSCs (Fig. 4D). The expression of smooth muscle-specific genes was determined using RT-qPCR analysis (Fig. 4E). The expression levels of Cx43, SM22α, desmin, and smoothelin genes were the highest in CE-SMC compared to those in other groups, suggesting that CE-SMC exhibited more mature SMC phenotypes.

Fabrication of cell-laden patch using PCL fibrous mat

To overcome the low mechanical properties of CE-SMC, a cell-laden fibrous structure was supplemented with a PCL strut for mechanical support. However, this solid structure would not be suitable for transplantation on the curved surface of the esophagus. Therefore, the PCL strut was replaced with a flexible PCL fibrous mat (Fig. S3A). PCL fibers or struts exhibited much stiffer mechanical properties than those of alginate fibers as determined by stress-strain curves (Fig. S3B). Young's modulus values (1.7 ± 0.2 and 2.0 ± 0.1 MPa) and maximum strength (8.6 ± 2.5 and 9.2 ± 1.7 MPa) were similar between PCL

fibers and struts (Fig. S3C). Owing to its flexible shape and appropriate mechanical property, a PCL fibrous mat was utilized to develop a cell-laden structure for *in vivo* testing.

Regeneration of esophageal defect using electrospun SMC patch in vivo

An esophageal defect is a disease in which there is a partial esophageal defect. Since CE-SMC exhibited mature SMC-like phenotypes, we examined the therapeutic effects of CE-SMC in an *in vivo* esophageal wound model. To confirm whether the CE-SMC patch can be used to repair smooth muscle injury, CE-SMC patches were transplanted into the esophageal defect model. To fabricate a patch for esophageal transplantation, PCL was first electrospun onto a drum collector to produce a PCL fibrous mat. Subsequently, SMCs were electrospun in five layers in the horizontal and vertical directions and cultured for 4 weeks prior to transplantation.

The esophagus is composed of inner and outer muscle layers, arranged in circular and longitudinal orientations, respectively. To mimic the structure of the esophagus, cell patches for transplantation were electrospun by stacking five layers in two directions (Fig. 5A). For transplantation, the fabricated patch was shaped with a biopsy punch with a 4 mm diameter (Fig. 5B (□)). To generate the rat esophageal defect model, the esophageal tissue was punctured with a 2 mm biopsy punch (Fig. 5B (□)), and the muscles around the esophagus and the inner mucosal layer were completely removed (Fig. 5B (□), (□)). Subsequently, the punctured section of the esophagus was covered with the fabricated patch and sutured (Fig. 5B (□)). At 2 weeks after the surgery, the tracheoesophageal tissue was dissected in the transverse direction (Fig. 5B (□); left arrow, trachea; right arrow, esophagus).

Histological analysis of the esophageal tissue was performed using H&E and Masson's trichrome staining. Thick fibrotic tissues and increased infiltration of immune cells were observed in the tissues transplanted with the control patch (Fig. 5C). By contrast, the esophagus transplanted with the CE-SMC patch exhibited a thick muscle layer and granulation tissue (Fig. 5D). To determine whether the transplanted patch promoted the regeneration of esophageal tissue, a detailed analysis was performed after immunostaining for vascular and smooth muscle markers (Fig. 6A, D). The number of blood vessels was found to be higher in rats with the CE-SMC patch than in those with the control patch (Fig. 6E). Furthermore, rats transplanted with the CE-SMC patch showed an abundance of newly formed blood vessels, indicating that vascularization was promoted by the CE-SMC patch. Consequently, CE-SMC patch transplantation significantly increased the levels of SM22α and vimentin expression relative to those of the control (Fig. 6B, C). These data indicate higher esophageal muscle regeneration in the SMC-patch group than in the control patch group.

To assess the effects of the CE-SMC patch on macrophage infiltration at the transplanted site, we performed CD68 immunostaining and identified macrophages as CD68 and DAPI double positive (Fig. 7A). The number of macrophages in the transplanted tissue was significantly increased in rats with the control patch and decreased by 50% in the CE-SMC patch group (Fig. 7B). These results suggest that the CE-SMC patch alleviated the immune response during esophageal reconstruction.

Discussion

Cell alignment is crucial for the reconstruction of smooth muscle tissues, such as those in the vasculature wall, intestinal tissue, or esophagus [39–41]; however, esophageal reconstruction with SMC alignment has not been reported [42, 43]. In the present study, cell electrospinning was used to direct cell alignment and elongation of cells. Compared with cell printing, cell electrospinning caused cell alignment in uniaxial direction. After cell electrospinning, electrospun MSCs and SMCs exhibited high cell viability, and the cells were attached along the electrospun fibers. Moreover, cell electrospinning induced longitudinal orientation of F-actin and stimulated the expression of extracellular matrix proteins in MSCs and SMCs compared with 3D bioprinting. Our observations suggest that CE is a promising technique that can control cell alignment to mimic the anisotropic architecture of native tissues. To replicate the gross anatomy of native tissues, aligned topography has been widely utilized to promote SMC alignment and elongation [46, 47]. For instance, Yi *et al.* found that in “an artificial wound” of the acellular fibrous region, most of the wound area was successfully covered by SMCs and transformed into an aligned, elongated morphology along the direction of the fibers [39]. In addition, increased cytoskeletal and nuclear aspect ratios have been reported as a critical factor in facilitating MSC-to-SMC differentiation, although the underlying mechanism of biophysical microenvironments affecting SMC differentiation is not clearly understood [48]. These results suggest that a unidirectional microenvironment is favorable for the development of engineered smooth muscle tissue to attain efficient cell-to-cell interactions and elongated morphology.

MSCs have shown a greater tendency to differentiate into SMCs on stiff (90 kPa–1500 kPa) substrates [49]. Herein, MSCs cultured on stiff substrates demonstrated increased calponin expression levels compared to those reported for MSCs cultured on soft substrates [37]. Additionally, the synergistic effects of a stiff surface and aligned topographical cues can alter mechanical deformations (nucleus and cytoskeletal elongation) into cellular biochemical responses [50], which, in turn, affect cellular functions and transcriptional activities [51]. In this study, alginate fibers exhibited a Young’s modulus of 116 ± 3 kPa and maximum strength of 3.5 ± 0.5 MPa. These results suggest that cells seeded on electrospun fibers preferentially differentiate into SMCs owing to appropriate mechanical properties and anisotropic cues. Moreover, the CE-SMC exhibited more increased proliferation than the CP-SMC, in contrast to similar proliferation rates between the CE-MSC and the CP-MS. Although the molecular mechanism involved in the increased proliferation of the CE-SMC is still unclear, it is likely that aligned topographic cues may be involved in the increased proliferation of the CE-SMC.

TGF-β has been reported to induce the differentiation of MSCs into SMCs [53]. TGF-β-treated MSCs exhibit SMC-like phenotypes but may also become myoblast, adipogenic, or osteogenic cells depending on environmental factors [53, 54]. Both α-SMA and calponin are significant markers of an SMC-like population because α-SMA is expressed in the early SMC developmental stage, whereas calponin is expressed exclusively in smooth muscle at the late stage of MSC-to-SMC differentiation. We found that α-SMA and calponin were sparsely expressed in CP-SMC, but not all the cell population became SMCs; however, the two proteins were highly expressed in CE-SMC. The expression levels of contractile markers

(Cx43, SM22α, desmin, and smoothelin) were significantly increased in CE-SMCs, further indicating SMC differentiation. The levels of these proteins are also reported to be upregulated in response to TGF-β, which is a regulator of SMC differentiation [37, 38]. Moreover, fibronectin and collagen I are generally known to be involved in ECM secretion. Therefore, the dominant expression of fibronectin and collagen I can be understood as evidence of differentiation. Furthermore, collagen IV acts not only as a major component of the ECM but also of the contractile SMC phenotype [55]. On the CE-SMC, the homogeneous distribution and aligned structure of fibronectin, collagen I, and collagen IV showed evidence of cell migration, proliferation, and SMC differentiation. Therefore, the cells on CE-SMC clearly showed evidence of SMC differentiation due to the synergistic effects of TGF-β and topographical cues.

As the esophagus enables peristalsis, the contractile phenotype is a critical factor for assessing the potential to restore contraction and relaxation following an esophageal injury. Our results indicate that a fibrous structure can serve not only as a mechanical support but also provide biophysical and biochemical cues. Esophageal injury can be caused by various factors such as inflammation, ulcer, stenosis, cancer, or physical impact [56], and in severe cases, an injury can cause esophageal defects. Small defects, perforation, and rupture of the esophagus are treated with sutures, but if the defect size is large, tissue transplantation is required. However, a practical method to effectively treat and regenerate the esophagus through tissue transplantation has not yet been developed. Consequently, many researchers have studied esophageal reconstruction through the transplantation of tissue scaffolds made from MSCs [57–59]. In this study, we transplanted the CE-SMC patch into an esophageal defect model to evaluate its clinical applicability. Although the SMC-scaffold was not transplanted in the esophagus in the form of a tube, but as a patch on a small defect area introduced by punching, we suggest an SMC-laden construct fabricated using CE as a useful resource that can be applied to esophageal reconstruction. PCL is a long-term stable polymer against biodegradation by hydrolysis, and it takes more than 2 years to complete degradation [60], implying usefulness of PCL for CE-mediated tissue engineering. The esophagus has an inner mucosal layer and an outer muscular layer that is mainly composed of the epithelium. While epithelial cells were not used for electrospinning in this study, we confirmed the tissue transplantation and regenerative potential of the CE-SMC-scaffold. In future studies, we will fabricate CE scaffolds using SMCs and epithelial cells and transplant them into small and large esophageal defects to confirm functional tissue repair, potentially expanding the therapeutic and clinical significance of SMCs.

Conclusion

This study presents a novel approach of anisotropic MSC-to-SMC differentiation *via* CE. In the electrospun fibers seeded with either MSCs or SMCs, both cell types showed high cell viability (> 90%). Furthermore, the cells displayed normal morphology marked by cytoskeletal structures (F-actin, fibronectin, collagen I, and collagen IV). Moreover, the electrospun SMC grew in a highly arranged, elongated morphology along the fiber direction. Additionally, the expression levels of SMC markers were greatly increased in CE-SMCs. When the CE-SMC scaffold was applied as a patch on a defective rat

esophagus, significant regeneration was observed in the esophageal defect model. These results suggest the potential of CE as a therapeutic approach for smooth muscle tissue regeneration.

Declarations

Acknowledgement

This study was supported by the MRC programs (NRF-2015R1A5A2009656) and grants from the National Research Foundation of Korea (NRF) funded by the Ministry of Science and ICT for Bio-inspired Innovation Technology Development Project (NRF-2018M3C1B7021997; NRF 2020R1A2C2011654).

Ethics approval and consent to participate

All animal experiments were reviewed and approved by the Institutional Review Board of Pusan National University Hospital (PNUH-2021-188). Human palatine tonsil tissues were isolated from patients after the patient's written informed consent and the study was approval by the Institutional Review Board of Pusan National University Hospital (1801-033-062).

Consent for publication

All authors have read and agreed to publish this manuscript.

Competing interests

The authors declared no potential competing interests with respect to the research, authorship, and/or publication of this article.

Data availability

The datasets generated during and/or analysed during the current study are available from the corresponding author on reasonable request.

Authors' contributions

Miji Yeo: Conceptualization, Methodology, Investigation, Writing – original draft.

Jung Won Yoon: Data curation, Formal analysis, Methodology, Writing – original draft.

Gyu Tae Park: Data curation, Formal analysis, Methodology

Sung-Chan Shin: Formal analysis, Investigation, Methodology

Young-Cheol Song: Formal analysis, Investigation, Methodology

Yong-Il Cheon: Formal analysis, Investigation, Methodology

Byung-Joo Lee: Data curation, Formal analysis, Investigation;

Geun Hyung Kim: Conceptualization, Methodology, Writing – review & editing, Supervision.

Jae Ho Kim: Conceptualization, Funding acquisition; Methodology, Writing – review & editing, Supervision.

References

1. Schlottmann F, Patti MG. Primary Esophageal Motility Disorders: Beyond Achalasia. Int J Mol Sci 2017, 18.
2. Londono R, Badylak SF. Regenerative Medicine Strategies for Esophageal Repair. Tissue Eng Part B Rev 2015, 21:393–410.
3. Arakelian L, Kanai N, Dua K, Durand M, Cattan P, Ohki T. Esophageal tissue engineering: from bench to bedside. Ann N Y Acad Sci 2018, 1434:156–163.
4. Pittenger MF, Discher DE, Peault BM, Phinney DG, Hare JM, Caplan AI. Mesenchymal stem cell perspective: cell biology to clinical progress. NPJ Regen Med 2019, 4:22.
5. Pittenger MF, Mackay AM, Beck SC, Jaiswal RK, Douglas R, Mosca JD, Moorman MA, Simonetti DW, Craig S, Marshak DR. Multilineage potential of adult human mesenchymal stem cells. Science 1999, 284:143–147.
6. Ohlstein B, Kai T, Decotto E, Spradling A. The stem cell niche: theme and variations. Curr Opin Cell Biol 2004, 16:693–699.
7. Kurpinski K, Lam H, Chu J, Wang A, Kim A, Tsay E, Agrawal S, Schaffer DV, Li S. Transforming growth factor-beta and notch signaling mediate stem cell differentiation into smooth muscle cells. Stem Cells 2010, 28:734–742.
8. Chen S, Lechleider RJ. Transforming growth factor-beta-induced differentiation of smooth muscle from a neural crest stem cell line. Circ Res 2004, 94:1195–1202.
9. Park WS, Heo SC, Jeon ES, Hong DH, Son YK, Ko JH, Kim HK, Lee SY, Kim JH, Han J. Functional expression of smooth muscle-specific ion channels in TGF-beta(1)-treated human adipose-derived mesenchymal stem cells. Am J Physiol Cell Physiol 2013, 305:C377-391.
10. Tay CY, Wu Y-L, Cai P, Tan NS, Venkatraman SS, Chen X, Tan LP. Bio-inspired micropatterned hydrogel to direct and deconstruct hierarchical processing of geometry-force signals by human mesenchymal stem cells during smooth muscle cell differentiation. NPG Asia Materials 2015, 7:e199-e199.
11. Tijore A, Behr JM, Irvine SA, Baisane V, Venkatraman S. Bioprinted gelatin hydrogel platform promotes smooth muscle cell contractile phenotype maintenance. Biomed Microdevices 2018, 20:32.
12. Zhou Q, Xie J, Bao M, Yuan H, Ye Z, Lou X, Zhang Y. Engineering aligned electrospun PLLA microfibers with nano-porous surface nanotopography for modulating the responses of vascular smooth muscle cells. J Mater Chem B 2015, 3:4439–4450.

13. Jiao A, Trosper NE, Yang HS, Kim J, Tsui JH, Frankel SD, Murry CE, Kim DH. Thermoresponsive nanofabricated substratum for the engineering of three-dimensional tissues with layer-by-layer architectural control. ACS Nano 2014, 8:4430–4439.
14. Kim SJ, Cho HR, Cho KW, Qiao S, Rhim JS, Soh M, Kim T, Choi MK, Choi C, Park I, et al. Multifunctional cell-culture platform for aligned cell sheet monitoring, transfer printing, and therapy. ACS Nano 2015, 9:2677–2688.
15. Ngandu Mpoyi E, Cantini M, Reynolds PM, Gadegaard N, Dalby MJ, Salmeron-Sanchez M. Protein Adsorption as a Key Mediator in the Nanotopographical Control of Cell Behavior. ACS Nano 2016, 10:6638–6647.
16. Huang J, Chen Y, Tang C, Fei Y, Wu H, Ruan D, Paul ME, Chen X, Yin Z, Heng BC, et al. The relationship between substrate topography and stem cell differentiation in the musculoskeletal system. Cell Mol Life Sci 2019, 76:505–521.
17. Teo BK, Wong ST, Lim CK, Kung TY, Yap CH, Ramagopal Y, Romer LH, Yim EK. Nanotopography modulates mechanotransduction of stem cells and induces differentiation through focal adhesion kinase. ACS Nano 2013, 7:4785–4798.
18. Jana S, Levengood SK, Zhang M. Anisotropic Materials for Skeletal-Muscle-Tissue Engineering. Adv Mater 2016, 28:10588–10612.
19. Cha SH, Lee HJ, Koh WG. Study of myoblast differentiation using multi-dimensional scaffolds consisting of nano and micropatterns. Biomater Res 2017, 21:1.
20. Yim EK, Reano RM, Pang SW, Yee AF, Chen CS, Leong KW. Nanopattern-induced changes in morphology and motility of smooth muscle cells. Biomaterials 2005, 26:5405–5413.
21. Parandakh A, Anbarlou A, Tafazzoli-Shadpour M, Ardeshirylajimi A, Khani MM. Substrate topography interacts with substrate stiffness and culture time to regulate mechanical properties and smooth muscle differentiation of mesenchymal stem cells. Colloids Surf B Biointerfaces 2019, 173:194–201.
22. Abolhasani S, Rajabibazl M, Khani MM, Parandakh A, Hoseinpoor R. The cooperative effects of micro-grooved topography and TGF-beta1 on the vascular smooth muscle cell contractile protein expression of the mesenchymal stem cells. Differentiation 2020, 115:22–29.
23. Zhou X, Nowicki M, Sun H, Hann SY, Cui H, Esworthy T, Lee JD, Plesniak M, Zhang LG. 3D Bioprinting-Tunable Small-Diameter Blood Vessels with Biomimetic Biphasic Cell Layers. ACS Appl Mater Interfaces 2020, 12:45904–45915.
24. Cui H, Zhu W, Huang Y, Liu C, Yu ZX, Nowicki M, Miao S, Cheng Y, Zhou X, Lee SJ, et al. In vitro and in vivo evaluation of 3D bioprinted small-diameter vasculature with smooth muscle and endothelium. Biofabrication 2019, 12:015004.
25. Sampson SL, Saraiva L, Gustafsson K, Jayasinghe SN, Robertson BD. Cell electrospinning: an in vitro and in vivo study. Small 2014, 10:78–82.
26. Ehler E, Jayasinghe SN. Cell electrospinning cardiac patches for tissue engineering the heart. Analyst 2014, 139:4449–4452.

27. Yeo M, Kim G. Fabrication of cell-laden electrospun hybrid scaffolds of alginate-based bioink and PCL microstructures for tissue regeneration. Chemical Engineering Journal 2015, 275:27–35.
28. Chen H, Liu Y, Hu Q. A novel bioactive membrane by cell electrospinning. Experimental cell research 2015, 338:261–266.
29. Yeo M, Kim GH. Anisotropically aligned cell-laden nanofibrous bundle fabricated via cell electrospinning to regenerate skeletal muscle tissue. Small 2018, 14:1803491.
30. Yeo M, Kim G. Micro/nano-hierarchical scaffold fabricated using a cell electrospinning/3D printing process for co-culturing myoblasts and HUVECs to induce myoblast alignment and differentiation. Acta Biomaterialia 2020.
31. Shin SC, Seo Y, Park HY, Jung DW, Shin TH, Son H, Kim YK, Lee JC, Sung ES, Jang JY, et al. Regenerative potential of tonsil mesenchymal stem cells on surgical cutaneous defect. Cell Death Dis 2018, 9:183.
32. Park GC, Song JS, Park HY, Shin SC, Jang JY, Lee JC, Wang SG, Lee BJ, Jung JS. Role of Fibroblast Growth Factor-5 on the Proliferation of Human Tonsil-Derived Mesenchymal Stem Cells. Stem Cells Dev 2016, 25:1149–1160.
33. Kim G, Park Ke. Alginate-nanofibers fabricated by an electrohydrodynamic process. Polymer Engineering & Science 2009, 49:2242–2248.
34. Bonino CA, Krebs MD, Saquing CD, Jeong SI, Shearer KL, Alsberg E, Khan SA. Electrospinning alginate-based nanofibers: From blends to crosslinked low molecular weight alginate-only systems. Carbohydrate Polymers 2011, 85:111–119.
35. Brun J, Lutz KA, Neumayer KM, Klein G, Seeger T, Uynuk-Ool T, Worgotter K, Schmid S, Kraushaar U, Guenther E, et al. Smooth Muscle-Like Cells Generated from Human Mesenchymal Stromal Cells Display Marker Gene Expression and Electrophysiological Competence Comparable to Bladder Smooth Muscle Cells. PLoS One 2015, 10:e0145153.
36. Chang S, Song S, Lee J, Yoon J, Park J, Choi S, Park JK, Choi K, Choi C. Phenotypic modulation of primary vascular smooth muscle cells by short-term culture on micropatterned substrate. PLoS One 2014, 9:e88089.
37. Rickel AP, Sanyour HJ, Leyda NA, Hong Z. Extracellular matrix proteins and substrate stiffness synergistically regulate vascular smooth muscle cell migration and cortical cytoskeleton organization. ACS Applied Bio Materials 2020, 3:2360–2369.
38. Weinbaum JS, Qi J, Tranquillo RT. Monitoring collagen transcription by vascular smooth muscle cells in fibrin-based tissue constructs. Tissue Engineering Part C: Methods 2010, 16:459–467.
39. Yi B, Shen Y, Tang H, Wang X, Li B, Zhang Y. Stiffness of aligned fibers regulates the phenotypic expression of vascular smooth muscle cells. ACS applied materials & interfaces 2019, 11:6867–6880.
40. Chen Y, Guo C, Manousiouthakis E, Wang X, Cairns DM, Roh TT, Du C, Kaplan DL. Bi-Layered Tubular Microfiber Scaffolds as Functional Templates for Engineering Human Intestinal Smooth Muscle Tissue. Advanced Functional Materials 2020, 30:2000543.

41. Chung E-J, Ju HW, Yeon YK, Lee JS, Lee YJ, Seo YB, Chan Hum P. Development of an omentum-cultured oesophageal scaffold reinforced by a 3D-printed ring: feasibility of an in vivo bioreactor. Artificial cells, nanomedicine, and biotechnology 2018, 46:885–895.
42. Chung EJ, Ju HW, Yeon YK, Lee JS, Lee YJ, Seo YB, Hum PC. Development of an omentum-cultured oesophageal scaffold reinforced by a 3D-printed ring: feasibility of an in vivo bioreactor. Artificial Cells Nanomedicine and Biotechnology 2018, 46:S885-S895.
43. Park SY, Choi JW, Park JK, Song EH, Park SA, Kim YS, Shin YS, Kim CH. Tissue-engineered artificial oesophagus patch using three-dimensionally printed polycaprolactone with mesenchymal stem cells: a preliminary report. Interactive Cardiovascular and Thoracic Surgery 2016, 22:712–717.
44. Tay CY, Wu YL, Cai PQ, Tan NS, Venkatraman SS, Chen XD, Tan LP. Bio-inspired micropatterned hydrogel to direct and deconstruct hierarchical processing of geometry-force signals by human mesenchymal stem cells during smooth muscle cell differentiation. Npg Asia Materials 2015, 7.
45. Olvera D, Sathy BN, Carroll SF, Kelly DJ. Modulating microfibrillar alignment and growth factor stimulation to regulate mesenchymal stem cell differentiation. Acta Biomaterialia 2017, 64:148–160.
46. Thakar RG, Cheng Q, Patel S, Chu J, Nasir M, Liepmann D, Komvopoulos K, Li S. Cell-shape regulation of smooth muscle cell proliferation. Biophysical journal 2009, 96:3423–3432.
47. Yim EK, Reano RM, Pang SW, Yee AF, Chen CS, Leong KW. Nanopattern-induced changes in morphology and motility of smooth muscle cells. Biomaterials 2005, 26:5405–5413.
48. Yeh Y-T, Wei J, Thorossian S, Nguyen K, Hoffman C, Del Álamo JC, Serrano R, Li Y-SJ, Wang K-C, Chien S. MiR-145 mediates cell morphology-regulated mesenchymal stem cell differentiation to smooth muscle cells. Biomaterials 2019, 204:59–69.
49. Park JS, Chu JS, Tsou AD, Diop R, Tang Z, Wang A, Li S. The effect of matrix stiffness on the differentiation of mesenchymal stem cells in response to TGF-β. Biomaterials 2011, 32:3921–3930.
50. Ingber DE. Tensegrity: the architectural basis of cellular mechanotransduction. Annual review of physiology 1997, 59:575–599.
51. Wang N, Tytell JD, Ingber DE. Mechanotransduction at a distance: mechanically coupling the extracellular matrix with the nucleus. Nature reviews Molecular cell biology 2009, 10:75–82.
52. Lee H, Kim G. Enhanced cellular activities of polycaprolactone/alginate-based cell-laden hierarchical scaffolds for hard tissue engineering applications. Journal of Colloid and Interface Science 2014, 430:315–325.
53. Liu Y, Deng B, Zhao Y, Xie S, Nie R. Differentiated markers in undifferentiated cells: expression of smooth muscle contractile proteins in multipotent bone marrow mesenchymal stem cells. Development, growth & differentiation 2013, 55:591–605.
54. Talele NP, Fradette J, Davies JE, Kapus A, Hinz B. Expression of α-smooth muscle actin determines the fate of mesenchymal stromal cells. Stem cell reports 2015, 4:1016–1030.
55. Ganesan MK, Finsterwalder R, Leb H, Resch U, Neumüller K, de Martin R, Petzelbauer P. Three-dimensional coculture model to analyze the cross talk between endothelial and smooth muscle cells. Tissue Engineering Part C: Methods 2017, 23:38–49.

56. Zwischenberger JB, Savage C, Bidani A. Surgical aspects of esophageal disease: perforation and caustic injury. Am J Respir Crit Care Med 2002, 165:1037–1040.
57. Catry J, Luong-Nguyen M, Arakelian L, Poghosyan T, Bruneval P, Domet T, Michaud L, Sfeir R, Gottrand F, Larghero J, et al. Circumferential Esophageal Replacement by a Tissue-engineered Substitute Using Mesenchymal Stem Cells: An Experimental Study in Mini Pigs. Cell Transplant 2017, 26:1831–1839.
58. Park H, Kim IG, Wu Y, Cho H, Shin JW, Park SA, Chung EJ. Experimental investigation of esophageal reconstruction with electrospun polyurethane nanofiber and 3D printing polycaprolactone scaffolds using a rat model. Head Neck 2021, 43:833–848.
59. Kim IG, Wu Y, Park SA, Cho H, Choi JJ, Kwon SK, Shin JW, Chung EJ. Tissue-Engineered Esophagus via Bioreactor Cultivation for Circumferential Esophageal Reconstruction. Tissue Eng Part A 2019, 25:1478–1492.
60. Sanchez-Gonzalez S, Diban N, Urtiaga A. Hydrolytic Degradation and Mechanical Stability of Poly(epsilon-Caprolactone)/Reduced Graphene Oxide Membranes as Scaffolds for In Vitro Neural Tissue Regeneration. *Membranes* 2018, 8.
61. Park H, Kim IG, Wu Y, Cho H, Shin JW, Park SA, Chung EJ. Experimental investigation of esophageal reconstruction with electrospun polyurethane nanofiber and 3D printing polycaprolactone scaffolds using a rat model. Head and Neck-Journal for the Sciences and Specialties of the Head and Neck 2021, 43:833–848.

Figures

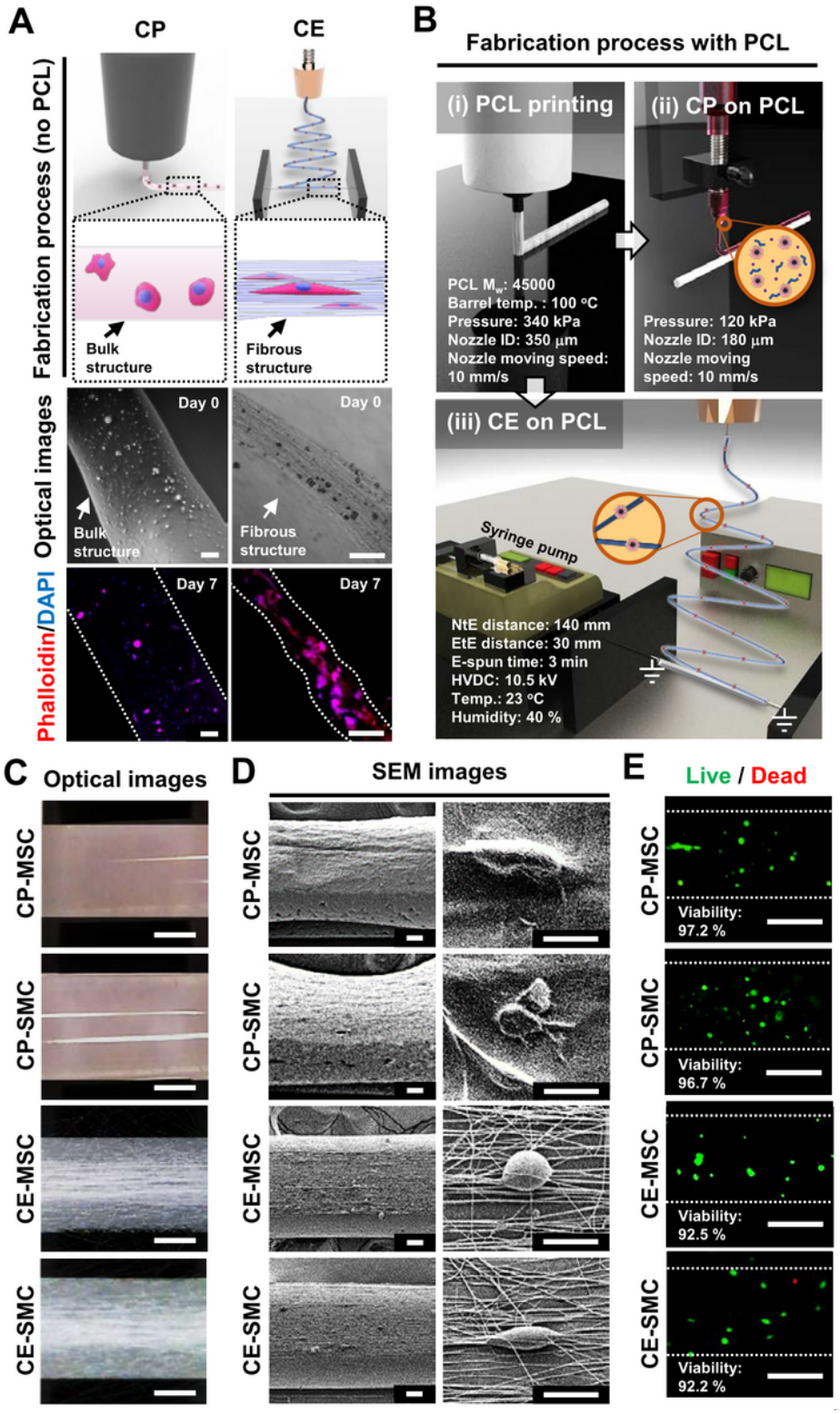

Figure 1

Fiber image of CP and CE with MSCs and SMCs. **A** Schematic representation of CP and CE fabrication without the supplement of a PCL strut. The fabrication procedures for CE and CP are shown in the upper panels, and the optical and fluorescent images (Phalloidin/DAPI double staining) are captured at day 0 and day 7 (lower panels; scale bar is 50 μm). **B** A schematic illustration of the PCL printing, CP, and CE processes. The fabricated scaffolds (CP-MSC, CP-SMC, CE-MSC, and CE-SMC) are represented as **C**

optical (scale bar is 100 μm), **D** SEM (scale bar is 40 μm), and **E** live/dead cell images (scale bar is 200 μm) at day 0.

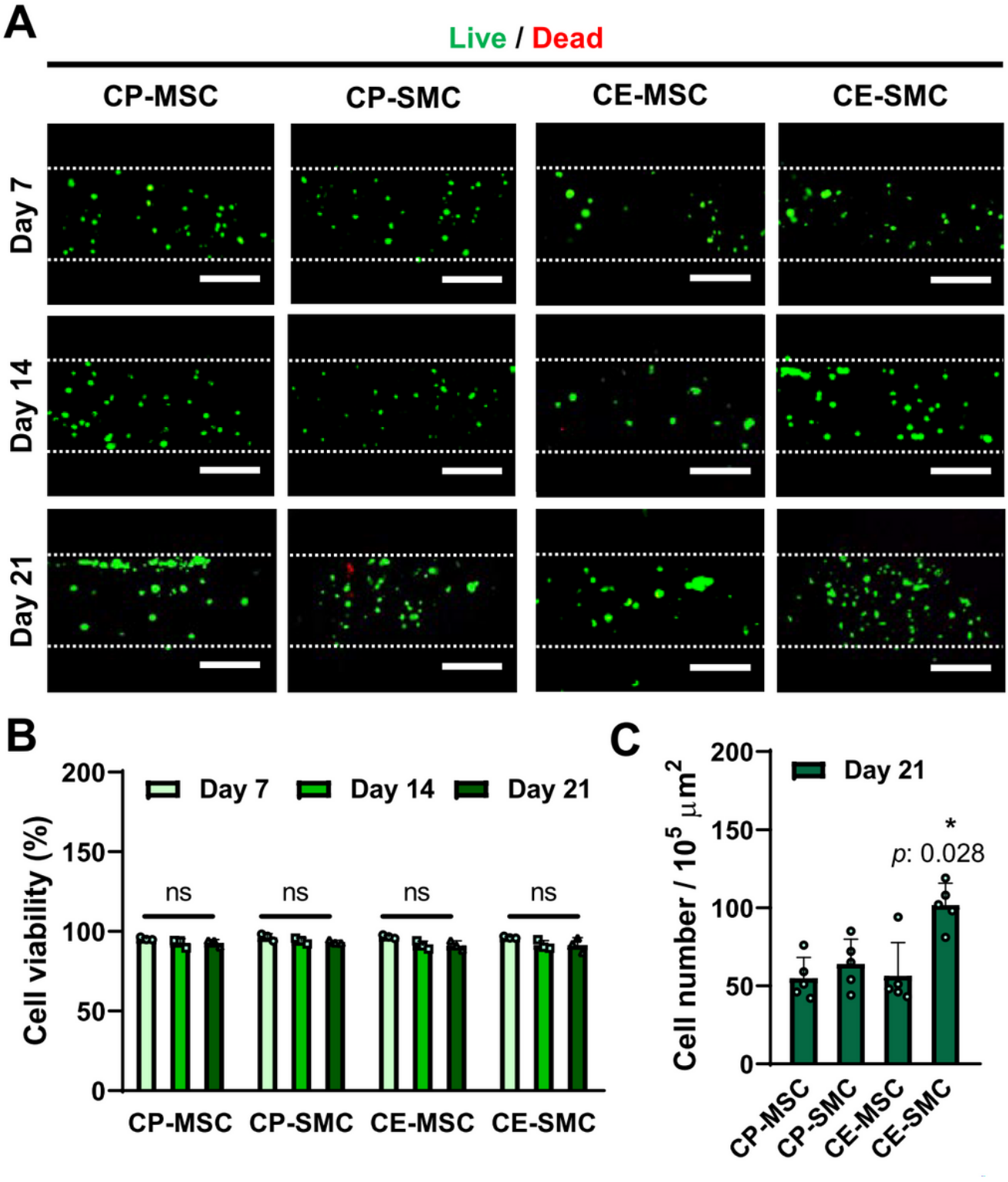

Figure 2

Effect of CP and CE on the viability and cell proliferation of MSCs and SMCs. **A** Live/dead cell images of CP-MSC, CP-SMC, CE-MSC, and CE-SMC cultured for various periods. Quantitative analysis of the

live/dead cell images with respect to **B** cell viability and **C** cell number. Scale bar is 200 mm.

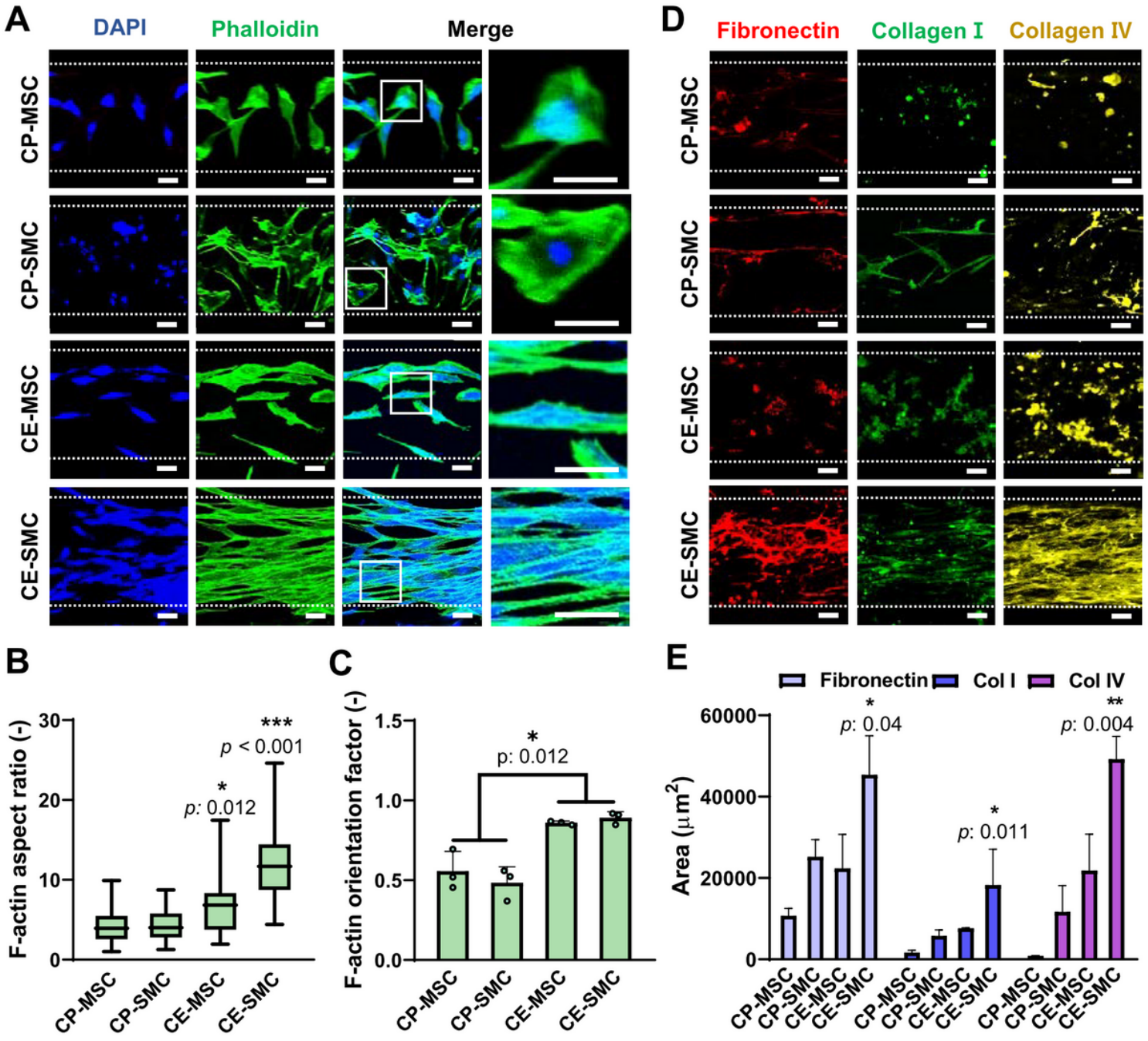

Figure 3

Effect of CP and CE on the arrangement of MSCs and SMCs. **A** Phalloidin/DAPI staining at 21 days and quantitative analysis of the **B** F-actin aspect ratio and **C** F-actin orientation factor. **D** Fluorescence images of fibronectin, collagen I, and collagen IV at 21 days and **E** quantitative analysis of area. Scale bar is 50 μm.

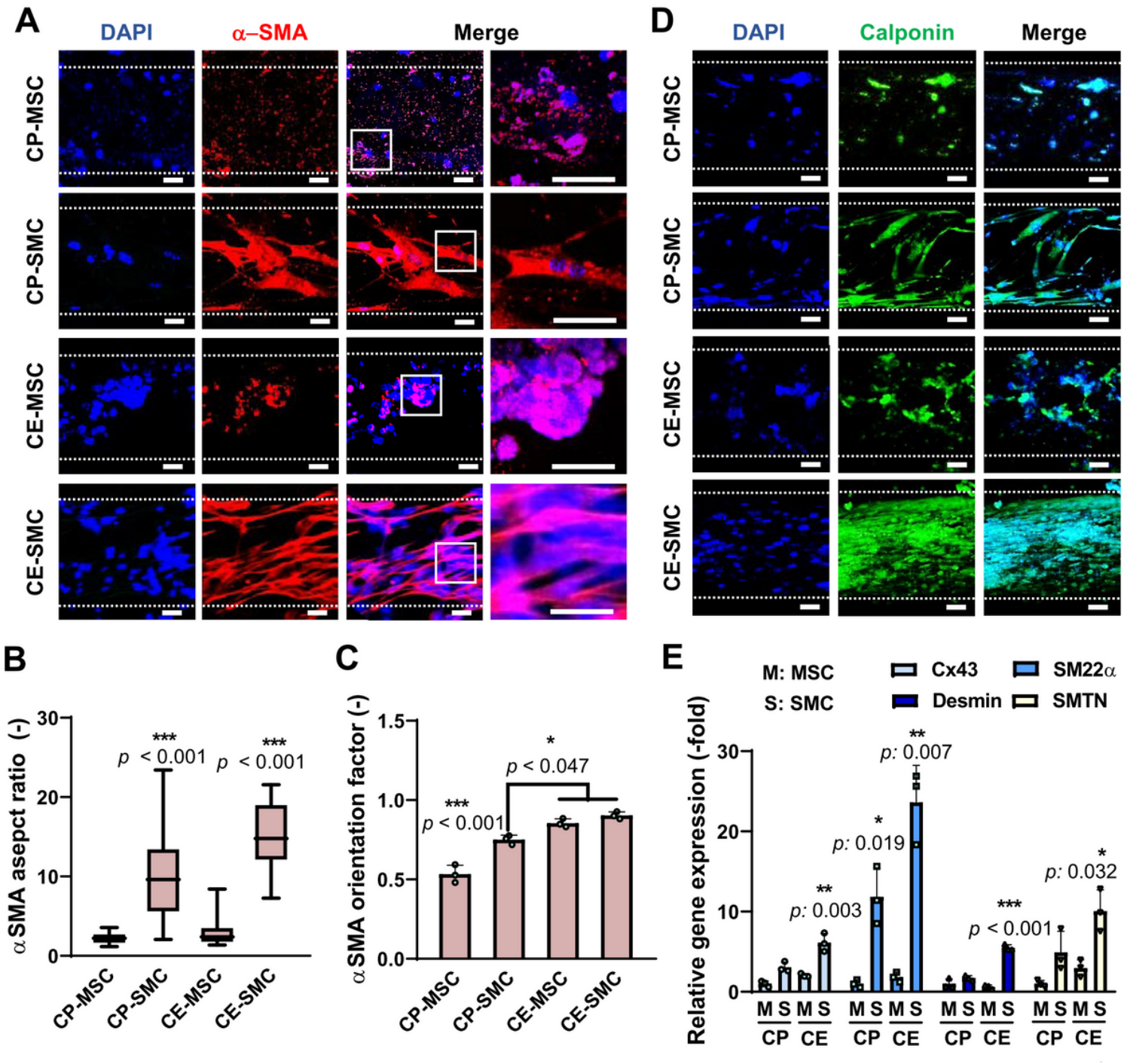

Figure 4

CE promotes a higher degree of maturation of SMCs than that of CP. **A** α-SMA/DAPI staining at 21 days and quantitative analysis of the **B** α-SMA aspect ratio and **C** α-SMA orientation factor. **D** Calponin/DAPI staining at 21 days and **E** analysis of relative smooth muscle-specific gene expression. *GAPDH* was used to normalize gene expression. Scale bar is 50 μm.

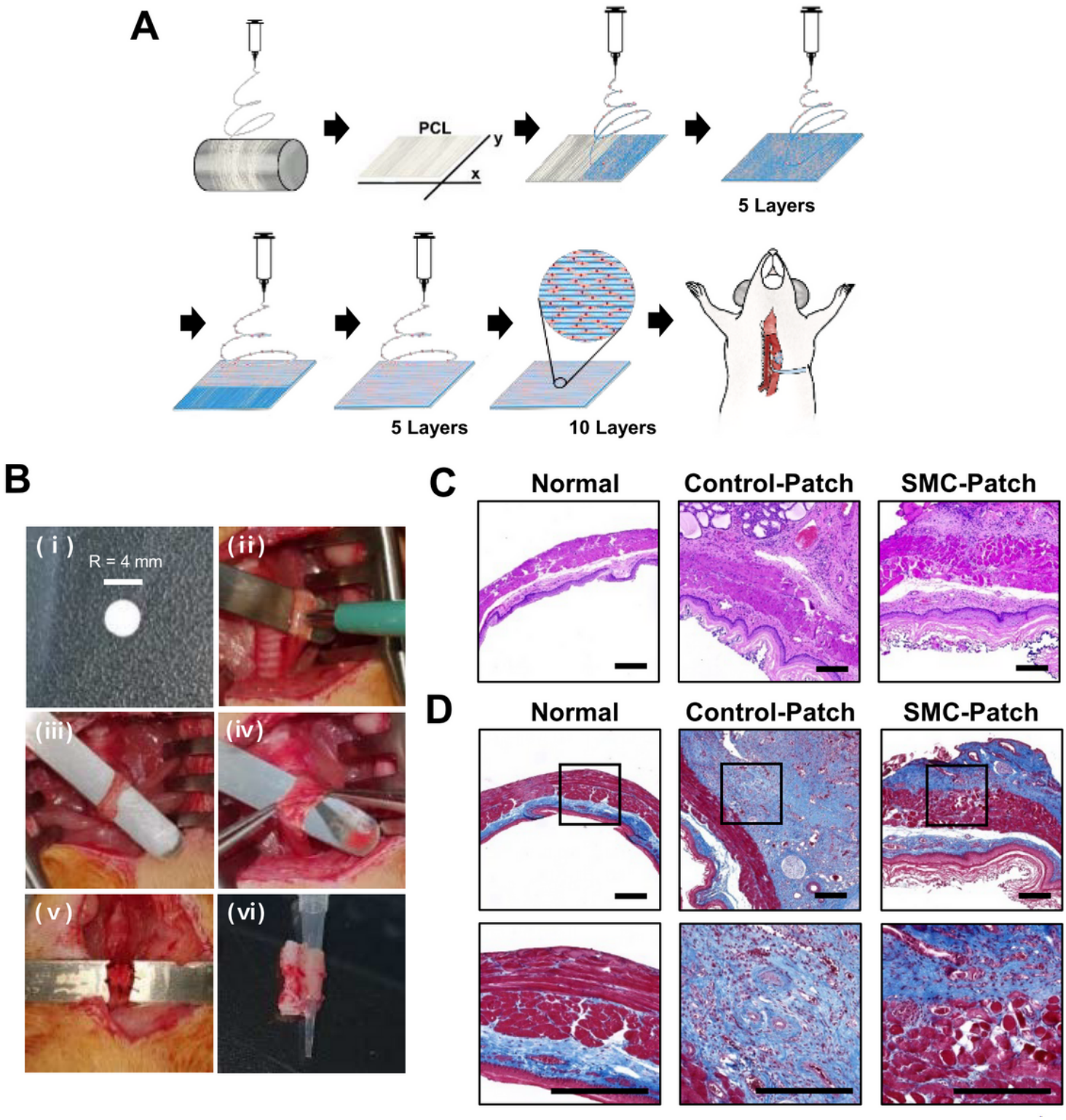

Figure 5

CE-SMC fabrication and transplantation of an SMC-patch to repair esophageal defect in a rat model. **A** A schematic illustration of the SMC electrospinning workflow for the fabrication of a CE SMC-patch for transplantation. **B** Representative images of the surgical procedure using which patch was transplanted in the esophageal defect rat model. Images of **C** H&E staining and **D** Masson's trichrome staining of the defective esophagus at 2 weeks after transplantation of either an SMC or cell-free patch and normal

esophagus. (Normal, without surgery; Control-Patch, cell-free construct; SMC-Patch, SMC-laden construct). Scale bar is 300 μm.

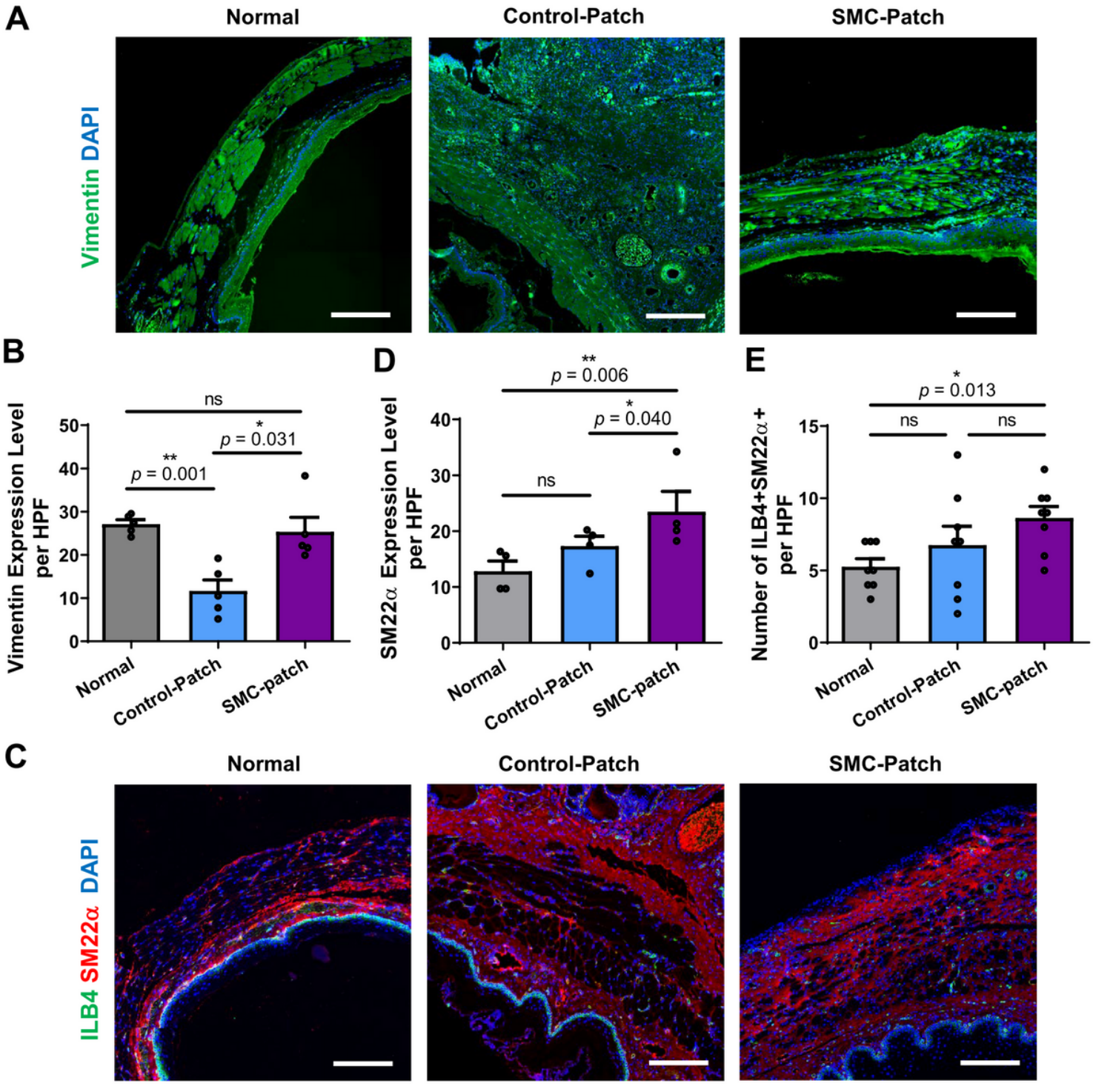

Figure 6

Neovascularization and regeneration of esophageal smooth muscles after patch transplantation in a defective esophagus model. Representative images of **A** vimentin, **C** ILB4 and SM22α immunostaining in a defective esophagus at 2 weeks after transplantation of either an SMC or cell-free patch and normal

esophagus. Quantitative analysis of **B** vimentin and **D** SM22α expression as measured by the fluorescence levels. **E** Quantitative analysis of ILB4 and SM22α expression levels was performed by counting the number of ILB4 and SM22α double-positive cells. (Normal, without surgery; Control-Patch, cell-free construct; SMC-Patch, SMC-laden construct). Scale bar is 200 μm.

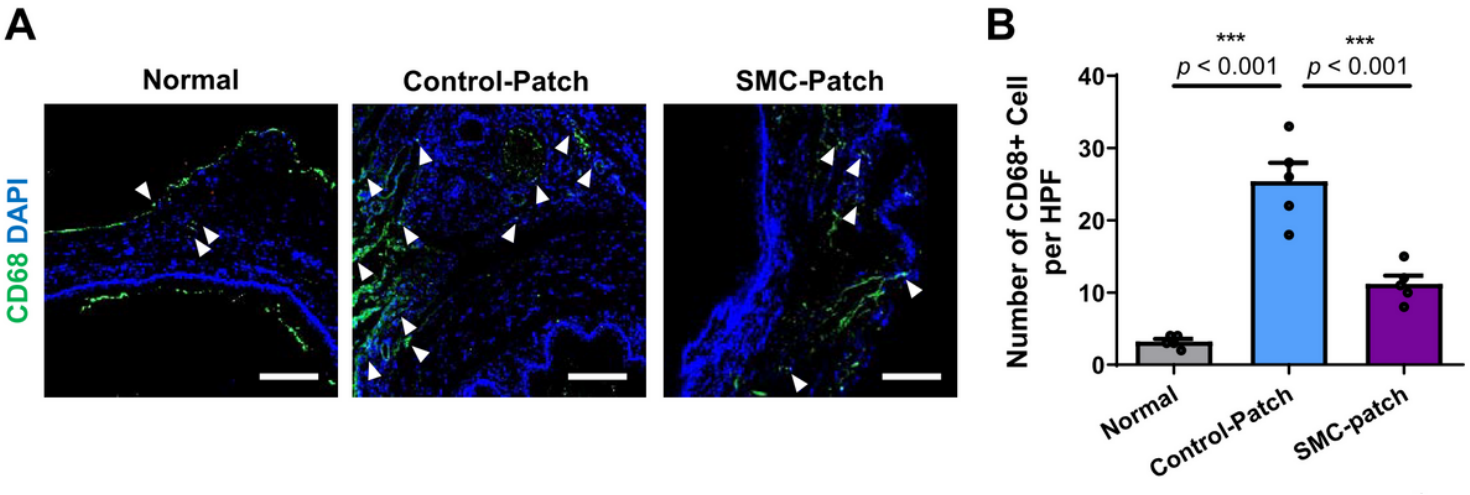

Figure 7

Regulation of the inflammation in esophageal tissue after SMC-patch transplantation in a defective esophagus model. **A** Representative images of CD68 immunostaining in a defective esophagus at 2 weeks after transplantation of either an SMC or cell-free patch and normal esophagus. **B** Quantitative analysis of macrophage infiltration in esophageal tissue was performed by counting the number of CD68 and DAPI double-positive cells. (Normal, without surgery; Control-Patch, cell-free construct; SMC-Patch, SMC-laden construct). Scale bar is 300 μm.

Supplementary Files

This is a list of supplementary files associated with this preprint. Click to download.

- GraphicAbstract.jpg
- SupplementaryInformationJNanobiothechfinalver.pdf